Journal of Japan Association for Earthquake Engineering, Vol. 21, No. 3, 2021

ESTIMATION OF VIBRATION CHARACTERISTICS OF KUZURYU RIVER BANK AND SUBSURFACE STRUCTURES BASED ON MICROTREMOR OBSERVATIONS

Masaki ITO[1], Keisuke KOJIMA[2] and Tomohiro MIZUNO[3]

[1] Technician, Department of Architecture and Civil Engineering, University of Fukui, Fukui, Japan, i-masaki@u-fukui.ac.jp
[2] Professor, Department of Architecture and Civil Engineering, University of Fukui, Fukui, Japan, k_kojima@u-fukui.ac.jp
[3] Engineer, Japan Pile Corporation, Tokyo, Japan, eritomomizuno@yahoo.co.jp

ABSTRACT: The Fukui Earthquake wreaked havoc on the Kuzuryu River bank. In this study, we obtained microtremor observations on the Kuzuryu River bank. An extended spatial autocorrelation (eSPAC) analysis was applied to the collected array observation data to estimate the Rayleigh wave-phase velocity. The predominant period of the bank was calculated from single-point three-component observation. S-wave velocity structures were back-analyzed based on the H/V spectrum. It was confirmed that the earthquake damages on the bank were harmonized with the back-analyzed structures.

Keywords: Fukui Earthquake, Kuzuryu River bank, Microtremor observation, Array observation, H/V spectrum

1. INTRODUCTION

The 1948 Fukui Earthquake (Mj = 7.1) caused unprecedented damage around the Fukui Plain with a total destruction rate ≥ 80%[1)]. This earthquake caused extensive damage to the Kuzuryu River bank over a wide area with vertical cracks, slope failure, and lateral over flow[2), 3)], that ultimately caused flood damages one month later. Even after the 2011 Tohoku Earthquake that occurred at the Pacific coast, more than 2,000 banks were damaged from Iwate Prefecture to Tokyo, and some of them diminished their function[4)]. Regarding the seismic resistance of river banks, performance checks and countermeasures have been in progress since the great damage to the Yodogawa River banks caused by the 1995 Southern Hyogo Prefecture Earthquake. However, these will take a long time to complete. To clarify the characteristics and seismic resistance of banks, in addition to boring, we will clarify continually the structure inside the bank by high-density surface waves and radar surveys in the presence of vibration. These methods generally require time and human resources that tend to be costly. Conversely, research studies have been published to clarify the underground structure using microtremors that are easy to measure. For example, Hata et al.[5)] conducted motion and tremor observations on the shoulders and tails of road banks. Based on the initial time difference of the S-wave, the transfer and cross-correlation functions determined the natural frequency and average S-wave

velocity of the bank. In this study, microtremor array and three-component observations were conducted in detail on the Kuzuryu River bank damaged by the 1948 Fukui Earthquake, and the transfer functions, H/V spectrum, and Rayleigh wave-phase velocities were calculated. At the same time, estimate herein the sedimentary structure of the levee body and the foundation ground based on them, and examine the correlation with the damages inflicted by the Fukui Earthquake.

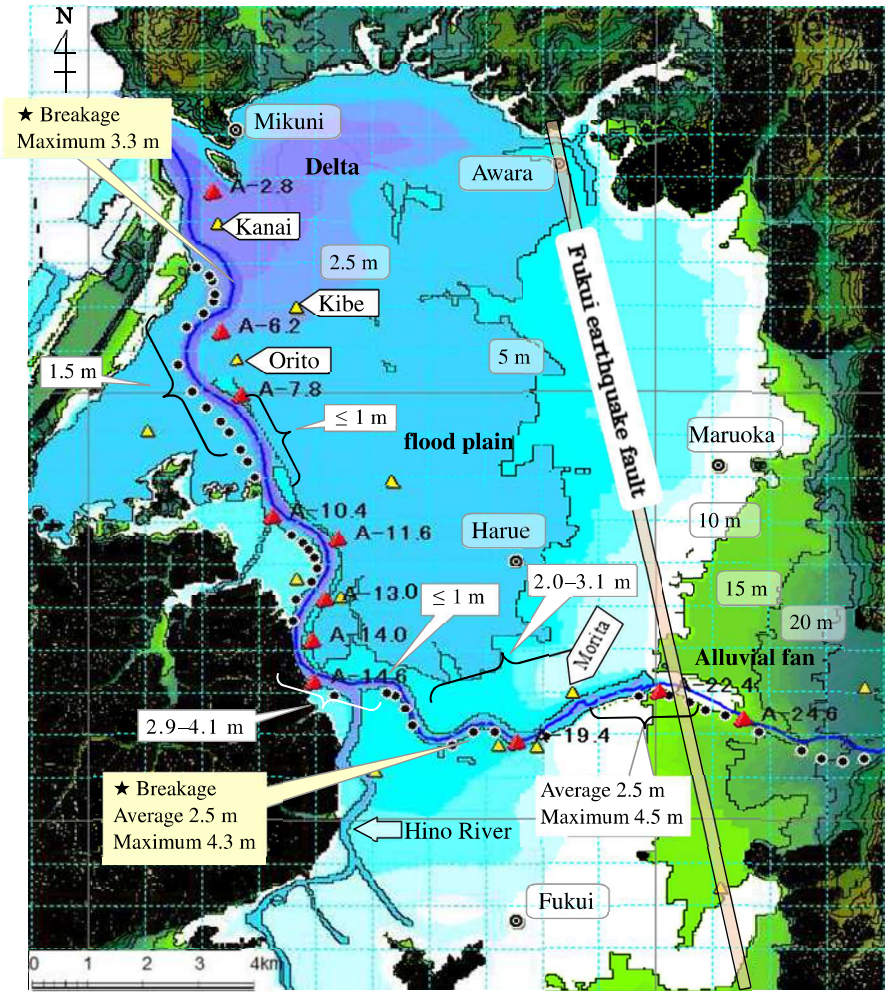

Fig. 1 Microtremor observation points, topography map and location of the Kuzuryu River

2. OUTLINE OF DAMAGE TO THE KUZURYU RIVER BANK DUE TO THE FUKUI EARTHQUAKE

Figure 1 shows the topographic map, the microtopographic distribution of the Fukui Plain, and the location of the Kuzuryu River. In the Fukui Plain, along the Kuzuryu River, fans, floodplains and deltas are distributed from the upstream side. An outline of the subsidence amount of the bank was based on the damage report of the Special Investigation Committee Hokuriku Earthquake[2)] is shown in Fig. 1 in a balloon. Figure 2 shows the subsidence of the foundation ground (G) and top parts (Top) of the right (R) and left banks (L) of the Kuzuryu River bank according to the distance from the estuary. The amount of subsidence of the foundation ground ranged from approximately 70 cm in the section from the estuary to approximately 18 km, but it decreased monotonously towards the upstream alluvial fan at

approximately 27 km. Conversely, even if the average subsidence was 1.5 to 2 m, a maximum of 4.5 m was documented near the estimated location of the Fukui Earthquake fault at 22 km, and 4.3 to 4.5 m at 14 km and 19.4 km away from the fault, respectively.

Owing to heavy rain that fell one month after the earthquake, the bank of Fukui City Tomyoji (19 km) shown in Fig. 1 (the plots of ★) collapsed along the left bank for 300 m. Damage levees caused severe secondary disasters, that included 7,000 houses, 1,900 hectares of land, and 2.4 m depth of flooding.

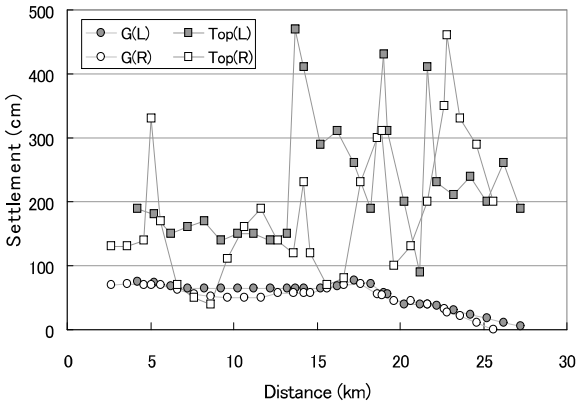

Fig. 2 Distribution of subsidence of foundation ground and levee body in Fukui Earthquake

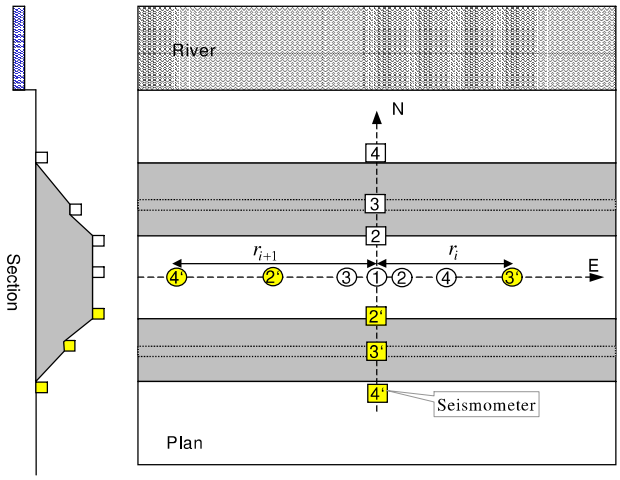

Fig. 3 Arrangement of setup for microtremor observations

3. MICROTREMOR OBSERVATIONS AT THE KUZURYU RIVER BANK

3.1 Microtremor observations

The microtremor observation points are plotted in Fig. 1. The plots of ▲ (big triangle) are the array observation points on the Kuzuryu River bank, and the plots of ● are the single-point three-component observation point. The array observation was conducted based on the selection of 11 points that were not open, as roads among the points at which there were boring data[6] that belonged to the Ministry of Land, Infrastructure and Transport. The array observation point was coded as A-7.8, wherein the A- is combined with the distance (km) from the estuary of the Kuzuryu River. A single-point three-component observation was conducted based on the selection of 47 points from an area within which it was judged that there was little traffic and disturbance every 400 m along the 4.0 km piles on the left bank of the Kuzuryu River. For microtremor observations, we combined the LE-3D/Lite seismometers, manufactured by Lennartz and an LS-8800 data logger, manufactured by Hakusan Industry. We set a sampling interval of 0.005 s and a duration of approximately 10 min.

Figure 3 shows the layout of the microtremor array observations acquired in this study in the plan and cross-sectional views. In the case of microtremor observations, the NS direction of the seismometer was set to the bank crossing direction (the riverside was assigned to the symbol N), and the EW direction was set to the longitudinal direction. The array observation in the longitudinal direction of the bank aims to obtain the Rayleigh wave-phase velocity using the extended spatial autocorrelation method (eSAPC method)[7]. The observed phase velocity was back-analyzed to obtain the S-wave velocity structure directly below the bank and foundation ground. For the microtremor array observations shown in Fig. 3

used four seismometers. Seismometer ① was fixed at the center of the top of the bank (defined as the origin). Seismometers ② to ④ were set along the E direction on the geometrical progression distances with the first term equal to 1 m and a common ratio equal to $-\sqrt{3}$. By conducting three simultaneous observations by changing the first distance, 18 combinations of the distance r between the two seismometers can be obtained within the range of 1 to 74 m ($\cong 27+27\sqrt{3}$) with little overlap. Therefore, we can evaluate the error function between the observed spatial autocorrelation coefficient and the Bessel function without bias. Hereinafter, this array observation will be referred to as linear extended array observation. In addition, to study the vibration characteristics of the bank, simultaneous observations along the transverse direction were conducted in which the seismometers were placed at the center of the top of the levee body (C), top (T), and middle (M) of the slope, and on the ground surface (G) beside the toe of the slope.

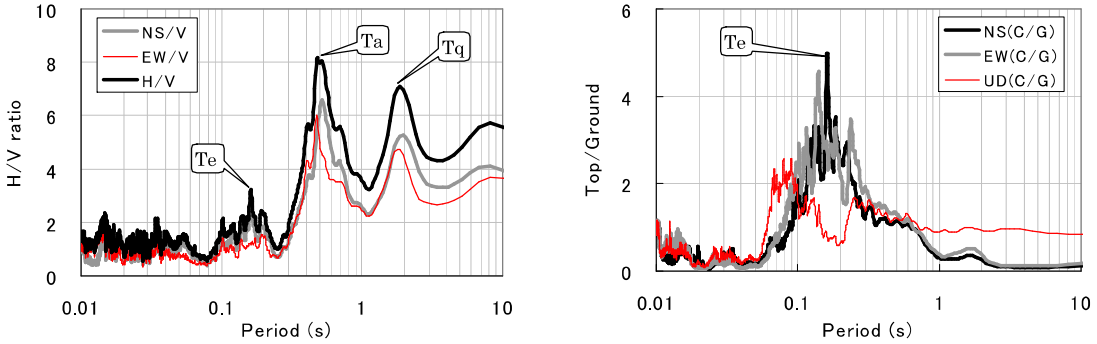

(a) H/V spectrum on center of levee body of observation point

(b) Transfer function between the center of levee body and the foundation ground

Fig. 4 H/V spectrum of the top of levee body, transfer function between the top of levee body and foundation ground

3.2 Predominant period of levee body and foundation ground

From the recorded data, sections of 40.96 s were extracted and 20.48 s was overlapped. The power of each segment was calculated, and approximately ten calm sections were selected in order of decreasing power, and Fourier analysis was performed to calculate the transfer function and H/V spectrum by applying cosine-type taper. Figure 4 shows the spectral characteristics of the simultaneous observation along the transverse direction point at 19.4 km near the location of the bank breakage due to heavy rainfall after the Fukui Earthquake. Figure 4(a) shows the spectral ratio of the NS, EW, and horizontal motion component H ($H=\sqrt{NS^2+EW^2}$) divided by the vertical motion component V. All spectral ratios have clear peaks at approximately 0.58 s and 1.8 s, respectively. Based on the results of microtremor observations in the Fukui Plain by the authors in the past[8),9)], these two peaks were inferred to be predominant periods owing to the alluvial soft layer and the lowermost quaternary layer, respectively. Hereafter, they are referred to as Ta and Tq, respectively. The same peak periods could be read in the H/V spectrum of the other array and single-point observation points shown in Fig. 1, but Tq was not found at some observation points near the foothill and on the alluvial fan. In those cases, Tq was read from the small peak based on the peak period of the adjacent point. Figure 4(b) shows the transfer function in each direction between the center of the top (C) of the bank and the foundation ground (G). In this figure, the existence of the peaks corresponding to Ta and Tq observed in the H/V spectrum of Fig. 4(a) cannot be confirmed because the vibration components due to the foundation

ground which are commonly observed at the top of the levee body and at the toe of the slope are canceled. Conversely, there is a clear peak at 0.16 s in the transverse direction (NS/V) and approximately 0.14 s in the longitudinal direction (EW/V). These are considered to correspond to the natural periods of the levee body and are called Te (H/H). The peaks corresponding to these peak periods can also be confirmed in the H/V spectrum in Fig. 4(a). Although not shown due to space limitations, we have confirmed that Te can be read from the H/V spectrum at other observation points.

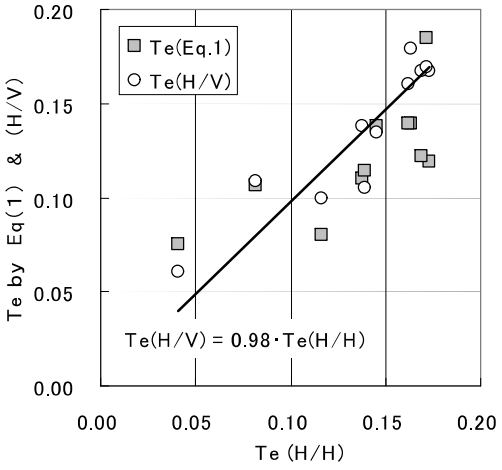

Fig. 5 Transfer function, H/V spectrum and comparison of natural period of the levee body obtained from Eq. (1)

The plots of ○ in Fig. 5 show a comparison of Te (H/H) in the transverse direction of the bank and the interpretation value Te (H/V) from the H/V spectrum at the transverse array observation point. Although there are variations, these values are closely matched. Nakamura and Nakano[10] proposed the natural frequency of the levee body from height H of the levee body, width B on top of the levee body, and the average S-wave velocity Vs by the following equation:

$$f_0 = 0.28 V_S H^{-0.84} B^{-0.13} \quad (1)$$

The plots of ■ in Fig. 5 show the natural period calculated by applying Eq. (1) to the average S-wave velocity calculated by the road bridge specification method[11] based on the boring information, and the N value of the levee body. These estimated values are slightly smaller than the values obtained from the transfer function, but the correlation is high. The ratios of the width of top to height on the observation points of the Kuzuryu River bank are distributed from 1.0 to 1.8 with an average of 1.3. Substituting B = 1.3H into the above equation yields the following equation:

$$f_0 = 0.27 \cdot V_S H^{-0.97} \cong V_S / (4H) \quad (2)$$

The relationship between this equation and Fig. 5 is the natural period of the Kuzuryu River bank is approximately represented by the law of a quarter wavelength. The vibration characteristics of the bank suggests that it can be approximated by the horizontal ground whose thickness is equal to the height of the levee body.

Figure 6(a) shows the predominant periods Ta and Tq due to the alluvial soft layer and quaternary layer of the foundation ground determined from the H/V spectrum of all stations as a distance from the

estuary (see Fig. 1). Both Ta and Tq tend to be small on the left bank (L) near the foot of the mountain. The Ta value exceeds 1 s on the downstream side, decreases monotonically toward the upstream side, and decreases to approximately 0.2 to 0.3 s 20 km upstream from the alluvial fan. Conversely, Tq ranges from 0.5 to 1.2 s up to 15 km in regions where the Kuzuryu River flows around the west side of the plain, but its values range from 1.6 to 2.3 s for distances ≥ 15 km in the plain. In the eastern plain for distances ≥ 23 km, within which is the estimated location of the Fukui Earthquake fault, there is a sharp decrease. The Fukui Earthquake fault is a left strike-slip fault with an eastern uplift, and the decrease in the dominant period Tq in the eastern part is consistent with the shallower basement in the eastern part, which is assumed from the fault motion. Figure 6(b) shows the distribution of the dominant period Te on the bank. Although Te tends to be small in the most downstream part, it varies from 0.1 to 0.2 s, which is considered to reflect the height of the levee body, soil used, construction quality, and variations in earthquake resistance.

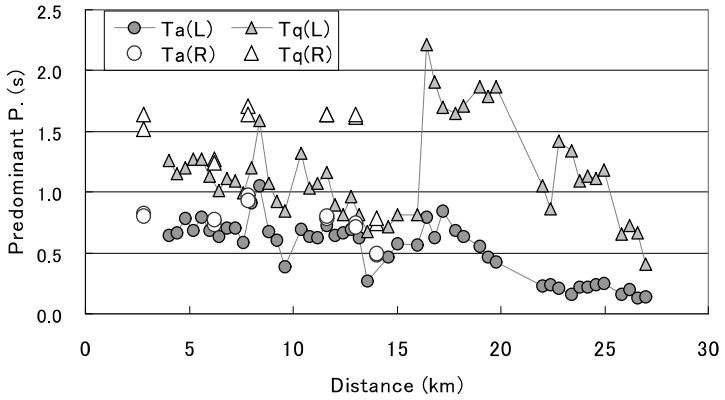

(a) Distribution of dominant period Ta and Tq of ground

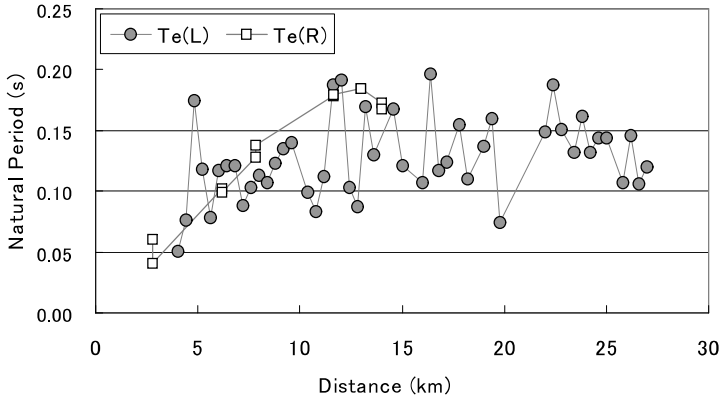

(b) Distribution of predominant period Te on the levee body

Fig.6 Predominant period of foundation ground and the bank determined from microtremor

4. CALCULATION OF RAYLEIGH WAVE-PHASE VELOCITY BASED ON OBSERVATIONS FROM THE LINEAR EXTENDED ARRAY

In the previous chapter, it was shown that the microtremor predominant period of the bank can be approximated by a structure in which the horizontal ground rests on the foundation ground with a thickness equal to the height of the bank. In this section, we assume that this approximation holds for microtremor propagation. Accordingly, the extended spatial autocorrelation method (eSPAC method)[7] is applied to the linear extended array observation. We assume that the spatial autocorrelation coefficients can be calculated by averaging the correlation coefficients of each segment of the microtremor recording, similar to the two-sided SPAC method (2sSPAC method) proposed by Morikawa et al.[12] .

In this study, the error $P(f)$ between the observed spatial autocorrelation coefficient ρ at frequency f and the Bessel function J_0 is evaluated by the following equation based on linear extended array observations,

$$P(f) = \sum_{i=1}^{N} w_i \left(\rho(f, r_i) - J_0\left(f\, r_i / \lambda(\omega)\right)\right)^2 / \sum_{i=1}^{N} w_i \tag{3}$$

where, r_i is the distance between the two microtremors, w_i is the weight that depends on the distance and the wavelength λ that is equal to one for $2\,r \leq \lambda \leq 10\,r$, and zero for $r \leq \lambda$ and $r \geq 50\,r$. It changed linearly between the two sections. In addition, N is the total number of combinations which is equal to $M \times {}_L\mathrm{C}_2$ when simultaneous observations with a number of L seismometers are performed M times. In the observation shown in Section 3.1, there are 18 ($= 3 \times {}_4\mathrm{C}_2$) types. The authors of this study[13] obtained the Rayleigh wave-phase velocity by applying the aforementioned method with a simulation waveform and a three-dimensional irregular ground model proposed by Cho et al.[14]. They confirmed that the results are comparable to the equilateral triangle arrangement and the cross arrangement. The compound matrix method[15] proposed by Saito and Kabasawa was used to calculate the theoretical H/V spectrum and phase velocity based on considerations of the Rayleigh and Love waves. When the H/V spectrum was calculated based on the research study of Tokimatsu and Arai[16], the Love wave power ratio was fixed at 0.7, regardless of the frequency, and the basic mode and the second-order higher-order mode were taken into consideration.

Figure 7 shows the relationship between the spatial autocorrelation coefficient of the vertical motion component and the distance r by the linear extended array in the longitudinal direction of the bank at A-13. The plots show the observed value (O) for each frequency, and curve (C) shows J_0 by the optimized phase velocity. The correlation between the observed spatial autocorrelation coefficient and the Bessel function is good, and the result shows that a phase velocity that can explain the observed oscillation characteristics is obtained. The plots of ○ in Fig. 8 are an example of the Rayleigh wave-phase velocity obtained by a linear extended array observation. At the points shown here, relatively smooth phase velocities with positive dispersion are required from approximately 1 Hz to approximately 12 Hz. The solid lines in the figure are phase velocities obtained by applying the SPAC method to the equilateral triangular array observations[8] with three different array radii that ranged from 4 m to 50 m at the locations indicated by the symbols ▲ in Fig. 1 (small triangles). As demonstrated, these markers were close to the array observation points. The array observations on the bank seem to produce phase velocities close to the usual observations made on the ground surface. The results obtained following the application of the extended SPAC method to eleven site observations are summarized in Table 1. In the same table, the markers of ○ indicate those with good correspondence to the equilateral triangle array observations. The markers of Δ indicate those for which continuous phase velocities with positive dispersion were obtained, but deviated from the equilateral triangle array, while the markers of × indicate those for which phase velocities were not calculated.

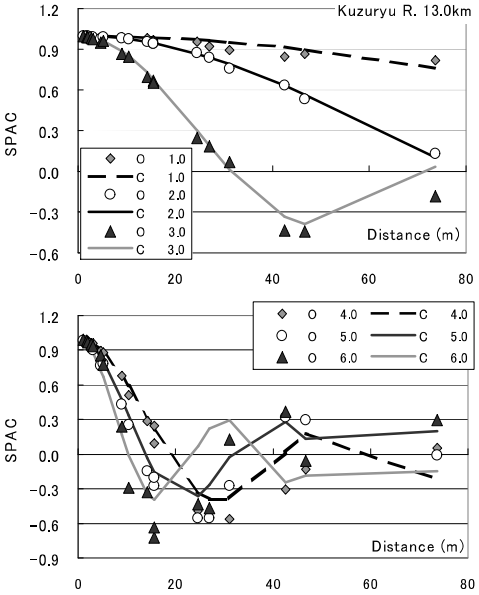

Fig.7 Comparison of spatial autocorrelation coefficients and Bessel function

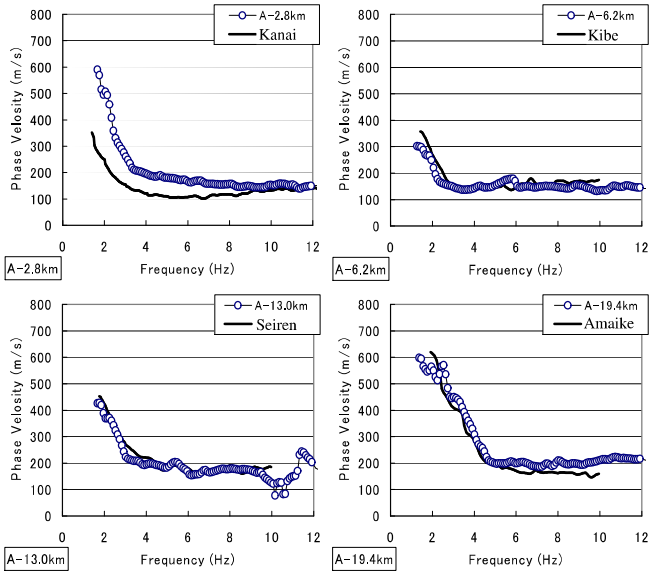

Fig.8 Comparison of Rayleigh wave phase velocities calculated from the linear extended array and circular array observation

Table 1 Phase velocity calculation results using the liner extended array

Points	2.8 km	6.2 km	7.8 km	10.4 km	11.6 km	13 km
Results	Δ	○	○	Δ	Δ	○
Points	14 km	14.6 km	19.4 km	22.4 km	24.6 km	
Results	○	Δ	○	×	Δ	

5. ESTIMATION OF STRUCTURE OF LEVEE BODY AND FOUNDATION GROUND BASED ON H/V SPECTRUM

5.1 Formulation of underground structure estimation scheme

The subsurface structure of the bank and foundation ground was estimated based on the H/V spectrum calculated from the single-point three-component observed every 400 m on the center point on the levee body of the Kuzuryu River bank array. The estimation of the underground structure was as follows; (1) the ground model consisted of five layers, which included the bank body, the alluvial soft layer (except for the sand and gravel layer in the alluvium where Vs was greater than 300 m/s), diluvial layer, and the seismic bedrock; (2) The density of each layer was known, and the P-wave velocity was linked to the S-wave velocity by the empirical formula by Kozaki et al.[17]; (3) The bank layer thickness was fixed to the surveyed value, and the S-wave velocity of the diluvium and tertiary layers are fixed at 580, 1800 and 3200 m/s. These were the average values[8] in the Fukui Plain; (4) From the above, the estimation targets were four S-wave velocities V_{SE} and V_{SA} of the bank and alluvium, and the thicknesses Ha and Hd of alluvial soft layer and diluvium; (5) The initial values of Ha and Hd were assumed to be the predominant periods Ta and Tq read from the H/V spectrum to the bottom of the alluvial soft layer and the natural

period due to the quaternary layer. The S-wave velocity of the alluvium was set to 170 m/s [8]. It was set to the value obtained by applying the law of a quarter wavelength; and (6) A search was conducted for the correction rates for the initial values of V_{SE}, V_{SA}, Ha and Hd that minimize the following objective function *J*.

$$J = \frac{1}{N_f}\sum_{i=1}^{Nf}\left[\log_{10} H/V_i^O - \log_{10} H/V_i^C\right]^2 + \sum_{j=1}^{N_f-1}\left[\frac{G_j^O - G_j^C}{2(N_f-1)}\right]^2 \rightarrow \text{minimum} \qquad (4)$$

where H/V_i^O and H/V_i^C were the observed and theoretical H/V spectrum, respectively, G_j^O and G_j^C are a slope terms binarized to -1 and 1 depending on whether the slope of the observed and the theoretical H/V spectrum were negative or greater than zero. The comparison period ranged from 0.05 to 4 s. A genetic algorithm (GA) was used for the search. The number of individuals was 30, the number of bits was 6, the number of generations was 20, the crossover probability was 0.6, the mutation probability was 0.05, and dynamic mutation and elite selection were considered.

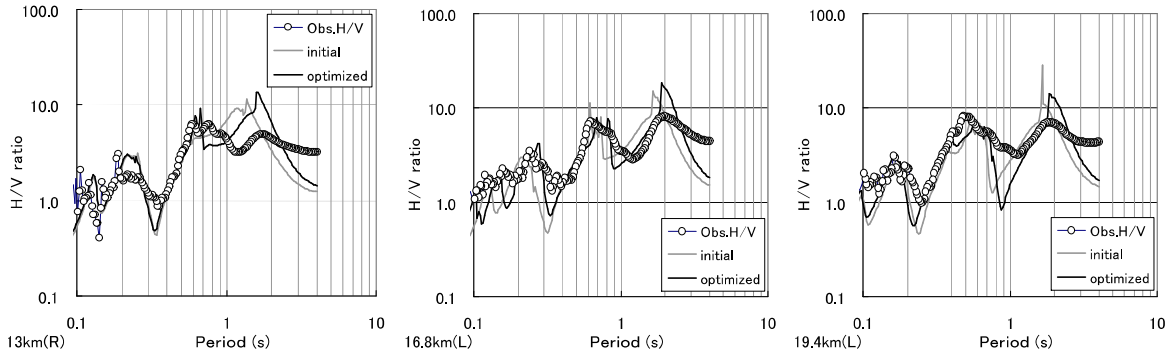

Fig. 9 Comparison of observed H/V and theoretical H/V based on the optimal ground model

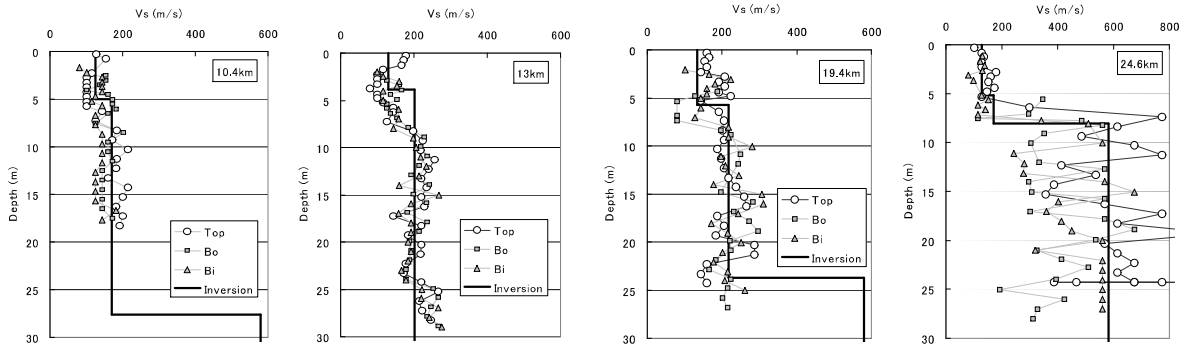

Fig. 10 Comparison of S-wave velocity and estimated structure by the N-values of the levee body and foundation ground

5.2 Correlation between estimated results of underground structure and Fukui Earthquake damage

Figure 9 shows a comparative example of the observed H/V spectrum and the theoretical H/V spectrum using the initial and the optimum ground models. The theoretical H/V spectrum based on the optimum ground model shows the peaks and troughs of the observation, except for the very short period band. It can be confirmed that the period reproduced well, and the amplitude value corresponded relatively well.

Figure 10 shows an example of a comparison between the S-wave velocity distributions of the levee body and foundation ground obtained by applying the method[11] of the road bridge specification for the N-value and the optimum S-wave velocity structural model. The N-value is plotted at three points: at the top of the levee body (Top), the riverside of bank (Bo), and the river landside of bank (Bi). It can be confirmed that the S-wave velocity of the levee body estimated from the microtremor is close to the average value of the estimated values by the N-value. Figure 11 shows the estimated S-wave velocity of the bank and the travel time average S-wave velocity based on the boring information for each distance from the estuary. The S-wave velocity (the plots with the markers ◊) of the bank was based on the boring information and was calculated with the use of the S-wave velocity at each depth and by averaging the travel time. The plots with the markers ■ are the average values of the three boring survey points. The plots with the markers ● are the estimated values based on the H/V spectrum, the plots with the large markers ○ are the cross-sections at which the boring survey was performed (array observation site), and the plots of small circles are the other three-component observation sites. From this figure, the S-wave velocities varies in the range of 100 to 180 m/s, and had large values in the estuary and alluvial fan upstream, and tended to be small in the floodplain area that crossed the plain. Estimates based on the H/V spectrum are 130 m/s in the downstream delta and around the foothills, 100 m/s in the midstream floodplain, and approximately 150 m/s in the fan-shaped areas. The smaller values in the midstream region are similar to those from the N values. This seems to suggest that silt, sand, cohesive soil, cohesive silt, and gravel soil, which are considered to be the main soils of deltas, flood plains, and alluvial fans, were used as dredging bank materials.

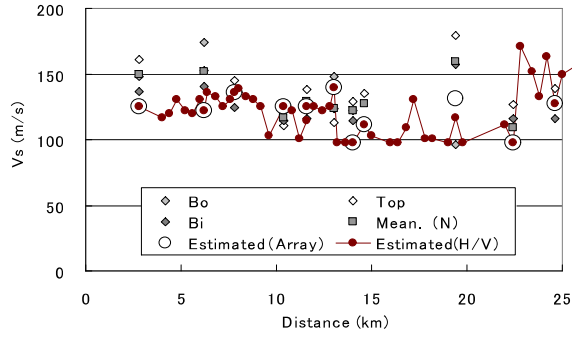

Fig.11 Comparison of S-wave velocity estimates of the levee body based on boring information and H/V spectrum

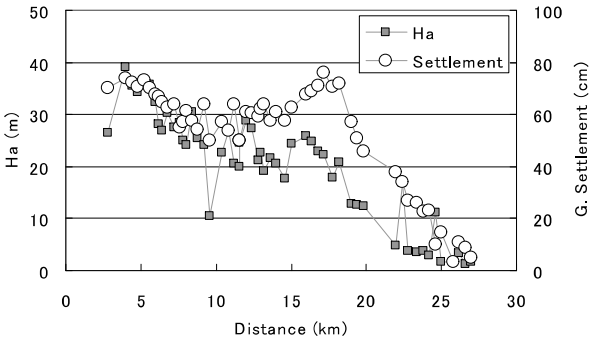

Fig.12 Estimated alluvial thickness and subsidence distribution of foundation ground

Figure 12 shows the estimated alluvial soft layer thickness Ha and the settlement of the bank foundation at each distance from the river mouth of the Fukui earthquake, based on microtremor. The amount of subsidence of the observation points shown in the plot with the ○ markers was calculated by spatial interpolation weighted by the reciprocal of the distance based on the survey results shown in Fig. 2. The thickness of the alluvial soft layer indicated by the markers ■ decreases monotonically from

approximately 40 m downstream, with the exception of the foothills at approximately 10 km and 14 km, it is estimated to be less than a few meters after 22 km within the fan-shaped region. In the area wherein the Kuzuryu River flows were almost parallel to the source fault, and at which the shortest distance of the fault was less than 15 km from the mouth of the river, the amount of subsidence gradually decreased as the alluvial soft layer decreased. Conversely, for distances > 15 km, the settlement increased temporarily up to 18 km as the soft layer increased and approached the hypocenter. Subsequently, the settlement did not increase even though the fault was close to the source, and decreased monotonically the thickness of the soft layer. The settlement of the foundation ground of the Kuzuryu River levee seemed to be different from the settlement trend of the levee itself, as shown in Fig. 2. This suggests that the influence of distance from the fault is small and the alluvial soft layer thickness is dominant.

6. CONCLUSIONS

Microtremor observations and single-point three-component observations of the Kuzuryu River bank were conducted, and the following results were obtained based on analyses. 1) From the H/V spectrum obtained by three-component observations at the top every 400 m, the natural period of the bank and the predominant period of the foundation ground based on the alluvium and the quaternary layer were deciphered. 2) By applying the extended SPAC method to the bank longitudinal direction survey line deployment array observations, the Rayleigh wave-phase velocities were calculated, and were found to be consistent with the phase velocities obtained from the surrounding circular array observations. 3) The average S-wave velocity of the bank and the thickness of alluvium and diluvium were optimized and calculated by inverse analysis based on the H/V spectrum. It was confirmed that the optimum ground model can reproduce the observed H/V spectrum well, was consistent with the boring information, and the subsidence of the foundation ground had a strong correlation with the estimated alluvial soft layer thickness.

From the above results, it is demonstrated that use of the method d described in this study, the vibration characteristics of the levee body and the approximate values of the ground structure of the levee-body-foundation can be obtained based on the single-point three-component observation at the top of the levee body. This is expected to be used for identifying places with a high risk of earthquake damage. In the future, it will be necessary to simultaneously observe multiple points of tremors in and around the levee body and examine the reproducibility of the vibration characteristics of the levee body foundation system based on the assumption of a horizontal sedimentary structure.

ACKNOWLEDGMENT

This research was conducted with the support of the Grant-in-Aid for Scientific Research (16K06464) and the Fukui Prefectural Collaborative Research Subsidy. Bank observations were graciously sponsored by the Fukui River National Highway Office.

REFERENCES

1) Hokuriku Earthquake Investigation Special Committee: *1948 Fukui Earthquake and Earthquake Investigation Report II Building Division*, Architectural Institute of Japan, 288 pp. 1–28, 1951 (in Japanese).
2) Hokuriku Earthquake Investigation Special Committee: *1948 Fukui Earthquake and Earthquake Investigation Report I Civil Engineering Division*, Architectural Institute of Japan, 183 pp. 73–82,1950 (in Japanese).
3) Central Disaster Prevention Council, Expert Committee on Succession of Disaster Lessons: *1948 Fukui Earthquake Report*, pp. 206–216, 2011 (in Japanese).

4) Japan Society of Civil Engineers River Bank Earthquake-Resistant Measures Emergency Review Committee: *Report on How to Proceed With Future River Bank Earthquake-Resistant Measures Based on the Great East Japan Earthquake*, pp. 1–11, 2011 (in Japanese).
5) Hata, Y., Ichii, K., Murata, A., Nozu, A., Miyajima, M. and Tsuneda, K.: An Evaluation of the Shear Wave Velocity Profile in a Road Embankment Using the Microtremor Measurement, *Journal of the Japan Landslide Society*, Vol. 48, No. 6, pp. 318–325, 2011 (in Japanese).
6) Fukui River National Highway Office, Kinki Regional Development Bureau, Ministry of Land, Infrastructure, Transport and Tourism: *River Current Ledger Appendix*, pp. 1–14, 2012 (in Japanese).
7) Ling, S. and Okada, H.: Extension of Spatial Autocorrelation Method in Microtremor Exploration Method, *Proceedings of the 89th SEGJ Conference,* pp. 44–48, 1993 (in Japanese).
8) Kojima, K. and Yasui, Y.: Estimation of S-wave Velocity Structure Down to the Seismic Bedrock of Fukui Plain Based on Microtremor Observation, *Journal of Japan Society for Natural Disaster Science*, Vol. 33, No. 4, pp. 359–374, 2015 (in Japanese).
9) Kojima, K. and Moto, K.: Estimation of S-wave Velocity Structure of Fukui Plain Based on Microtremoer Array Observation, *Journal of Japan Society of Civil Engineers*, Vol. 68, No. 1, pp. 98–109, 2012 (in Japanese).
10) Nakamura, Y. and Nakano, S.: Analysis of Changes in Natural Frequency with Bank Shape and Estimation Method of Physical Property Values, *The 43rd Japan Society of Civil Engineers Annual Meeting Proceedings*, No. 1, pp. 1172–1173, 1988 (in Japanese).
11) Japan Road Association: *Road Bridge Specification / Explanation V Seismic Design*, pp. 25–27, 2002 (in Japanese).
12) Morikawa, H., Ohori, M. and Iiyama, K.: A Study on Stochastic Properties of Auto-Correlation Coefficients for Microtremor Data Simultaneously Observed at Two Sites, *Journal of Japan Association for Earthquake Engineering*, Vol. 10, No. 2, pp. 89–106, 2010 (in Japanese).
13) Cho, I., Ohori, M., Kojima, K. et al.: Benchmark Test of Fine Movement Array Analysis Part 2. Phase velocities by SPAC methods, *Summaries of Technical Papers of Annual Meeting,* Architectural Institute of Japan, Vol. Structure II, pp. 339–340, 2017 (in Japanese).
14) Cho, I., Kamibayashi, H., Ohori, M. and Nagano, M.: Numerical Experiments on the Applicability of Various Microtremor Exploration Methods to Irregular Ground Structures (Part 1 Application Example of SPAC/CCA Method in Step/Inclined Base Structure Model), *Summaries of Technical Papers of Annual Meeting,* Architectural Institute of Japan, Vol. Structure II, pp. 1111–1112, 2016 (in Japanese).
15) Saito, M. and Kabasawa, H.: Computations of Reflectivity and Surface Wave Dispersion Curves for Layered Media 2. Rayleigh Wave Calculations, *Geophysical Exploration*, Vol. 46, No. 4, pp. 283–298, 1993 (in Japanese).
16) Tokimatsu, K. and Arai, H.: Effects of Rayleigh to Love Wave Amplitude Ratio on Microtremor Horizontal to Vertical Spectral Ratio, *Journal of Structural and Construction Engineering*, Architectural Institute of Japan, Vol. 63, No. 511, pp. 69–75, 1998 (in Japanese).
17) Kitunezaki, C., Goto, N., Kobayashi, Y., Ikawa, T., Horike, M., Saito, T., Kuroda, T., Yamane, K. and Okuzumi, K.: Estimation of P- and S- Wave Velocities in Deep Soil Deposits for Evaluating Ground Vibrations in Earthquake, *Journal of Japan Society for Natural Disaster Science*, Vol. 9, No. 3, pp. 1–17, 1990 (in Japanese).

(Original Japanese Paper Published: September, 2019)
(English Version Submitted: December 2, 2020)
(English Version Accepted: January 14, 2021)